



Contents lists available at ScienceDirect

Scripta Materialia

journal homepage: [www.elsevier.com/locate/scriptamat](http://www.elsevier.com/locate/scriptamat)

## Transient liquid-phase bonded 3D woven Ni-based superalloys

Dinc Erdeniz<sup>a,\*</sup>, Keith W. Sharp<sup>b</sup>, David C. Dunand<sup>a</sup>

<sup>a</sup> Department of Materials Science and Engineering, Northwestern University, 2220 Campus Drive, Evanston, IL 60208, USA

<sup>b</sup> SAERTEX USA, LLC, 2200-A Mt. Holly-Huntersville Road, Huntersville, NC 28078, USA

### ARTICLE INFO

#### Article history:

Received 26 March 2015

Revised 2 June 2015

Accepted 13 June 2015

Available online xxx

#### Keywords:

Nickel alloys

Pack cementation

Liquid-phase sintering

Microstructure

Mechanical properties

### ABSTRACT

Architected Ni-based superalloy scaffolds were fabricated by three-dimensional weaving of ductile Ni–20Cr (wt.%) wires followed by gas-phase alloying with aluminum and titanium via pack cementation. Bonding of neighboring wires occurs at necks that are formed by solid-state diffusion or by formation of a transient-liquid phase. Three-point bending tests of the superalloy weaves, after homogenization and aging to achieve a  $\gamma/\gamma'$  structure, show that, as bonding between wires increases, the materials withstand higher stresses and strains before onset of damage.

© 2015 Acta Materialia Inc. Published by Elsevier Ltd. All rights reserved.

Architected cellular materials [1–8], such as honeycombs [4], trusses [5], and wire-based structures [6–8], offer a combination of low density and high specific strength, stiffness, permeability, and surface area. These materials have periodic structures that can be designed by using topological optimization models to enhance the desired properties [9–11]. One example is 3D woven metal structures, fabricated from Cu or Ni–Cr wires, that are topologically optimized to provide improved permeability in preferred directions with minimal loss in stiffness for thermo-structural applications [8]. Such cellular materials are of interest for extreme environments, since increased permeability allows for active cooling and results in prolonged service life, or even enables material use, at elevated service temperatures and stresses. A number of studies have been published in the area of periodic cellular nickel-based superalloys, none, however, using topological optimization tools [12–14]. The main reason for the limited number of existing studies is the difficulty in the processing of such superalloy architected structures. Particularly, processing of wire-based structures are very challenging due to three manufacturing obstacles: (i) superalloy wires, especially below 500  $\mu\text{m}$  diameter, are difficult to draw, and hence not widely available through suppliers, (ii) if drawn, they are not sufficiently ductile to withstand the bending angles required for weaving, and (iii) if woven, the contact points must be bonded to reach the full potential of mechanical properties, which is difficult due to the

presence of oxide layers at the wire surface and low diffusivity, limiting the extent of solid-state bonding.

In a recent study, we reported the fabrication of topologically optimized Ni–Cr–Al superalloy structures produced using 3D textile processes [7,8]. Ni–20Cr (all compositions are given in wt.% hereafter) wires were 3D woven or 3D braided, taking advantage of the room-temperature ductility of these wires, and subsequently aluminized via pack cementation [7], a chemical vapor deposition process that has been widely used to create aluminate coatings on Ni-based superalloys for corrosion protection [15–17]. Aluminized 3D woven structures were then homogenized into Ni–Cr–Al alloys and aged for the precipitation of  $\gamma'$  particles, which are responsible for the high temperature creep resistance of superalloys. Simultaneously, the Ni–Cr–Al wires bonded by solid-state diffusion at their contact points during pack aluminization and homogenization [7]. In the present study, we demonstrate that Al and Ti can be co-deposited by pack cementation onto woven Ni–20Cr structures, which are then homogenized and aged to create Ni–Cr–Al–Ti superalloys where both Al and Ti act as  $\gamma'$  formers. We further show the bonding of the wires via the formation of a transient-liquid phase (TLP) due to the presence of Ti and evaluate the bending properties of the bonded and non-bonded structures.

Materials used in this study are non-crimp 3D orthogonal woven structures fabricated from soft-annealed Chromel A wires (Ni–20Cr–1Si–0.05Fe, labeled Ni–20Cr in the following) with a diameter of 202  $\mu\text{m}$  (32 gauge). A detailed description of the weaving process is given in Ref. [7] and the particular architecture used in the present work is labeled as “optimized weave,” in which

\* Corresponding author at: 2220 Campus Drive, Cook Hall 2036, Northwestern University, Evanston, IL 60208, USA.

E-mail address: [d-erdeniz@northwestern.edu](mailto:d-erdeniz@northwestern.edu) (D. Erdeniz).

topological optimization selected wire positions that are left vacant to increase material permeability. Woven samples, cut to a length of 72 mm, a width of 12 mm, and a thickness of 3.5 mm (corresponding to 11 wire layers), were buried in a pack mixture consisting of 57 wt.%  $\text{Al}_2\text{O}_3$  powders (20–50  $\mu\text{m}$  particle size) as filler, 30 wt.% Ti powders (99.5% purity, –325 mesh) and 10 wt.% Raney Ni precursor powders (Ni–50 wt.% Al, 150  $\mu\text{m}$  particle size) as sources, and 3 wt.%  $\text{NH}_4\text{Cl}$  powders (100  $\mu\text{m}$  particle size) as activator, with all powders procured from Alfa Aesar. At elevated temperature, the activator decomposes and reacts with the source powders to create a mixture of titanium and aluminum chloride gas, which subsequently deposits the metallic atoms onto the substrate [18,19]. Approximately 40 g of pack was poured in a steel retort, where the internal pressure rises at elevated temperatures,

and the cut specimen was placed at the center of the retort. The inner wall of the steel retort was spray-coated with boron nitride to minimize contamination. The retort was placed at the water-cooled end of a tube furnace that was heated to 1000 °C. After flushing the furnace tube with Ar for 15 min, the retort was pushed into the hot zone of the furnace, where it was held for 30 or 60 min. The retort was then pulled back to the water-cooled end of the tube and cooled there for 15 min. The specimens were removed from the pack and ultrasonicated in acetone for 2 h to remove all pack remnants. Samples cut from each specimen were vacuum-encapsulated in quartz tubes and heat-treated for homogenizing (1100–1200 °C, 48 h), solutionizing (1200 °C, 2 h), and aging (900 °C, 12 h). All heat-treatments were terminated with water quenching.

Samples were mounted in epoxy and prepared via standard metallographic techniques. An etchant composed of 33 vol.% deionized water, 33 vol.% acetic acid, 33 vol.% nitric acid, and 1 vol.% hydrofluoric acid was used to reveal the  $\gamma'$  precipitates. Microstructural and chemical analyses were conducted with an optical microscope and a scanning electron microscope (SEM) equipped with an energy dispersive X-ray spectrometer (EDS). Flexural behavior of the aged samples was evaluated via three-point bending tests with a 50 mm span, following ASTM-D970 and using a crosshead speed of 5 mm/min.

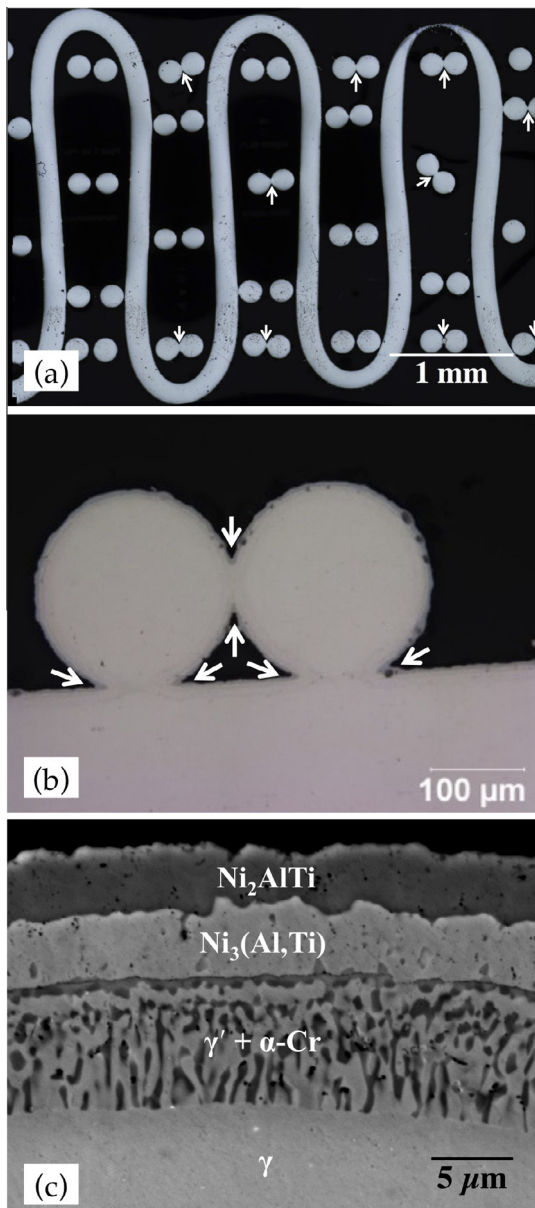


**Fig. 1.** (a) Optical micrograph showing polished cross-section of Ni–20Cr woven structure alumino-titanized at 1000 °C for 60 min with a total Al + Ti gain of 6 wt.%. Arrows mark the solid-state bonded necks between the wires. (b) Optical micrograph showing a higher magnification image of solid-state bonded necks, where sharp cusps are visible (arrows). (c) SEM image showing the structure of the coating consisting of three layers: outer –  $\text{Ni}_2\text{AlTi}$ , intermediate –  $\text{Ni}_3(\text{Al,Ti})$ , and inner – Cr-rejection in  $\gamma'$  matrix.

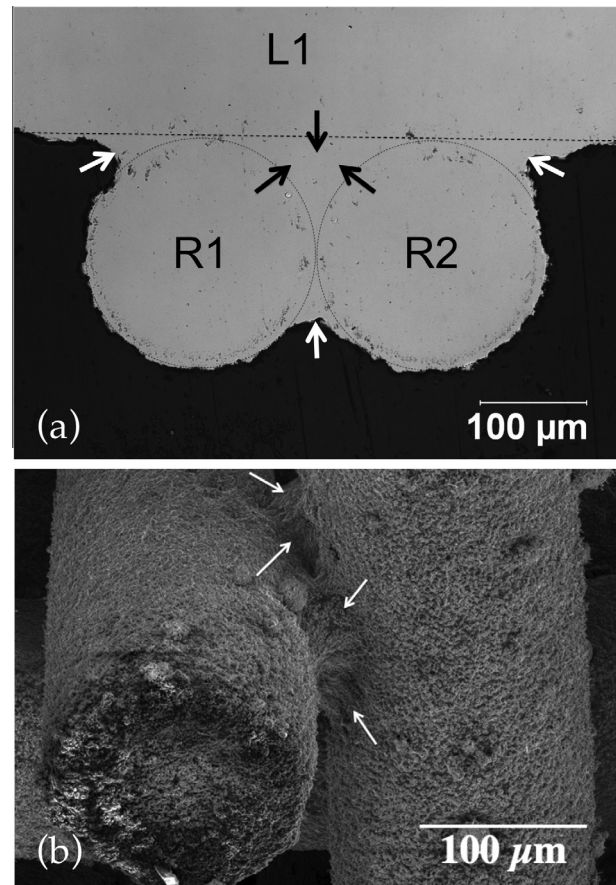


**Fig. 2.** (a) Optical micrograph showing cross-section of three wires (two radial labeled R1 and R2, one longitudinal labeled L1) which were TLP-bonded together in a Ni–20Cr weave that was alumino-titanized at 1000 °C for 30 min and homogenized/TLP-bonded at 1200 °C for 48 h. The outline of the original wires is shown with dotted lines, and the solidified liquid phase in the necks is marked with arrows. (b) SEM image of the same sample showing necks, marked with arrows, between two orthogonal wires.

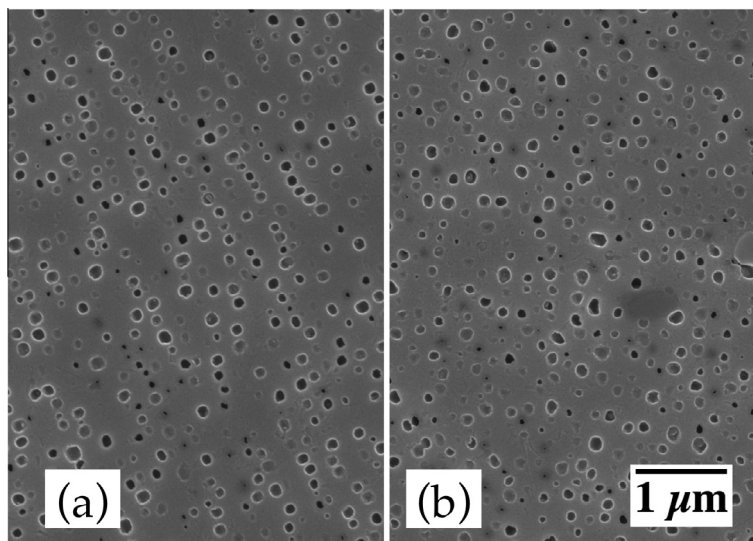


**Fig. 3.** SEM micrograph of etched  $\gamma/\gamma'$  microstructure of Ni–20Cr–3Ti–1Al woven structure, (a) center of a wire and (b) neck between wires. The sample was aluminotitanized at 1000 °C for 1 h, TLP-bonded at 1120 °C for 1 h, homogenized at 1100 °C for 24 h, solutionized at 1200 °C for 2 h, and aged at 900 °C for 12 h.

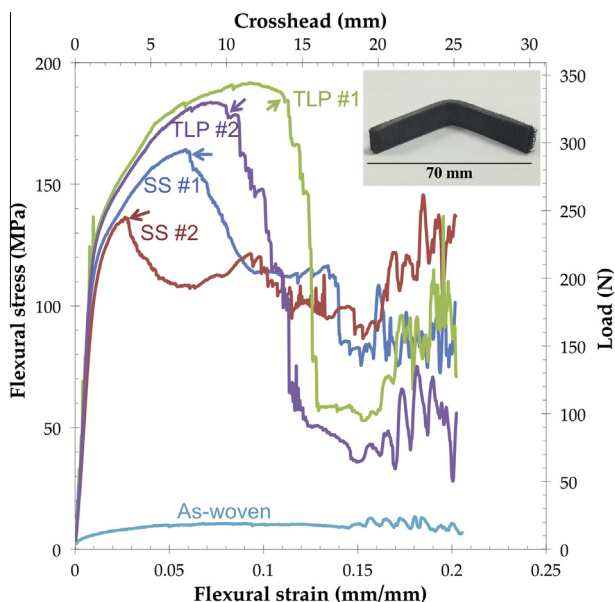


**Fig. 4.** Three-point bending stress–strain curves of Ni–20Cr–3Ti–1Al woven structures after solid-state (SS) bonding or transient-liquid phase (TLP) bonding and aging at 900 °C for 12 h to create a  $\gamma/\gamma'$  microstructure. Numbers 1 and 2 refer to repeat samples. For comparison, a curve for the Ni–20Cr weave is also shown (as woven: unalloyed and unbonded). Inset – deformed TLP-bonded sample.

The 3D woven Ni–20Cr structures, with a wire volume fraction of 32.7%, were pack-cemented for 30 min and 60 min at 1000 °C resulting in a weight gain of 4.5 and 6 wt.%, respectively. Fig. 1(a) shows a low-magnification optical micrograph of a Ni–20Cr woven structure coated by pack cementation at 1000 °C for 60 min, where the arrows mark bonding necks between wires. These necks formed in the solid-state when the wire volumes increased due to Al- and Ti-deposition. As a result, wires in contact with, or positioned very close to, each other impinged as they grew by Al- and Ti-deposition, forming necks at contact points. Similar behavior was observed during pack aluminization (without Ti) of Ni–20Cr weaves in our previous study [7]. Fig. 1(b) shows a higher magnification optical micrograph of the same sample, where sharp cusps are visible at the necks, indicating that surface diffusion is slow

compared to the gas-phase Al- and Ti- co-deposition rates, as also observed for Al-deposition in Ref. [7]. The SEM image shown in Fig. 1(c) reveals a three-layer coating structure: (i) a surface layer consisting of the  $\text{Ni}_2\text{AlTi}$  phase, (ii) a middle layer with  $\gamma'\text{-Ni}_3(\text{Al,Ti})$  phase composition, and (iii) an inner layer showing a mixture of Cr precipitates and  $\gamma'$  matrix phase. This third layer was formed by Cr rejection during the growth of the two other layers due to the limited solubility of Cr in the  $\text{Ni}_2\text{AlTi}$  and  $\text{Ni}_3(\text{Al,Ti})$  phases. The phase formation sequence shows some similarities with a study conducted by Nogorani et al. [19], where they co-deposited Al and Ti on Ni–10Co–8Cr–6Mo–6Al–4Ta–1Ti–0.1C (wt.%) superalloy coupons at various temperatures (850–1050 °C) using packs with a range of Ti/Al mass ratios (0.5–3.5). At 1000 °C, the coatings on samples treated in packs with a Ti/Al mass ratio of 2.5 and 3.5 (as compared to the ratio of 6 used in the present study) consisted of  $\text{Ni}_2\text{AlTi}$  along with  $\text{Ni}_2\text{Ti}$  and NiAl. Discrepancies between the two studies can be attributed to different sample composition, geometry, and specific surface area, which significantly affect the deposition rates, and hence, the phases formed.

As-coated samples were subsequently heat-treated to homogenize the wires by interdiffusion and create an alloy with uniform composition within the wires. Fig. 2(a) shows a sample coated for 30 min and homogenized at 1200 °C for 48 h. The coating layers completely disappeared and uniform distribution of the elements was confirmed with EDS line-scans. Importantly, extensive bonding was also achieved between the wires [20]. Fig. 2(a) shows three wires: two with radial cross-sections (marked as R1 and R2) and one with longitudinal cross-section (marked as L1). It is clear that the gaps between the wires were completely filled and there are no sharp cusps, as was observed with the solid-state bonded sample shown in Fig. 1(b). This indicates formation of a transient-liquid phase (TLP) during the homogenization process; the liquid wicked into the small gaps between the wires (as marked with arrows) due to the capillary effect before solidifying as the composition homogenized. Consequently, three wires with a composition of Ni–20Cr–2.5Ti–0.5Al were achieved, with substantial necks of the same composition. Further SEM observations showed that the necks formed throughout the specimen where wires were in contact with, or close to, each other. A representative SEM image given in Fig. 2(b) illustrates the appearance of the necks, as marked with arrows. Creation of a transient-liquid phase is expected given a



known eutectic at 904 °C in the Ni–Al–Ti ternary system [21]. TLP bonding of Ni-based alloys is a well-established method, using a B, Mn, and/or Si-containing interlayer which is added in the form of foils, powders, pastes, or coatings [22]. In these cases, the bonding layer includes a significant amount of the above elements, which can have detrimental effects if they diffuse into the bonded parts. This presents a critical challenge when the diffusion distance is particularly small, i.e., 100 µm for the woven wires discussed here. Hence, the TLP bonding technique developed in our study, where Al- and Ti-are added in the gas phase, provides a crucial advantage as the interlayer contains elements which are beneficial for superalloys in terms of enhancing oxidation resistance and creating  $\gamma'$  precipitates necessary for creep strength. Upon homogenization, the bonded wires and the necks achieve the same composition by interdiffusion, and thus have the same mechanical and chemical properties.

The SEM image in Fig. 3(a) shows the  $\gamma'$  precipitate microstructure of a Ni–20Cr–3Ti–1Al woven specimen, which formed after alumino-titanizing at 1000 °C for 1 h, TLP bonding at 1120 °C for 1 h, homogenizing at 1100 °C for 24 h, solutionizing at 1200 °C for 2 h, and aging at 900 °C for 12 h. This image was taken from a region close to the center of a wire at the core of a weave and was representative of the whole sample. The precipitates have a near-cuboidal morphology, typical of Cr-, Al-, and Ti-containing Ni-based superalloys [23], with a volume fraction of 15% and an average size of  $105 \pm 15$  nm. Fig. 3(b) shows a similar micrograph taken from a neck between two wires in the same sample. The presence of  $\gamma'$  precipitates with the same size and volume fraction as in the center of a wire (Fig. 3(a)) confirms the EDS results showing identical compositions in both the wires and their necks.

Stress–strain curves in Fig. 4 show the flexural behavior of TLP-bonded Ni–20Cr–3Ti–1Al samples (heat-treatment procedure given above) along with as-woven Ni–20Cr and solid-state (SS) bonded Ni–20Cr–3Ti–1Al woven structures (homogenized/bonded at 1100 °C for 24 h, solutionized at 1200 °C for 2 h, and aged at 900 °C for 12 h) for comparison purposes. Two samples for each processing condition were tested. The curves are characterized by elastic deformation, a yield point, a strain hardening region, a first major stress dip where failure starts (marked with arrows), and a plateau over a 10–15% strain range that is followed by serrations, which indicate failures of individual or groups of wires and/or necks. The TLP-bonded structures reached ~25% higher maximum strength than the SS-bonded structures, which is attributed to the higher bonding efficiency, in terms of the neck numbers and volumes, achieved with the TLP technique. The main difference between the sample pairs (TLP #1 vs. TLP #2 and SS #1 vs. SS #2) is the strains at which the failure started. This is probably due to variations in number and area of necks in each sample, which is directly related to the spacing between wires in the as-woven material and can be improved during the 3D weaving process.

Also, both TLP samples started failing at higher strains and stresses than the two SS-bonded samples, once again indicating the higher efficiency of bonding between wires. This translates into absorbed energy values (as measured by integration of the stress–strain curve up to 10% strain) of 17 and 16 MJ m<sup>-3</sup> for TLP bonded samples and 13 and 11 MJ m<sup>-3</sup> for SS-bonded samples (#1 and #2, respectively), while the energy absorbed by the as-received sample was only 0.9 MJ m<sup>-3</sup>. The resulting stress drop upon initial failure, followed by a plateau region at the 10–15% strain range, is higher for the TLP-bonded samples than the SS-bonded ones. This is potentially due to larger stress accumulations on the TLP-bonded weaves during the test, which caused a higher level of damage once the necks and wires started failing.

The authors acknowledge financial support from the Defense Advanced Research Projects Agency under award number W91CRB1010004 (Dr. Judah Goldwasser, program manager). They also thank Profs. Kevin Hemker, Timothy Weihs, and James Guest (Johns Hopkins University) for useful discussions.

## References

- [1] R. Lakes, *Nature* 361 (1993) 511.
- [2] Y. Brechet, J.D. Embury, *Scr. Mater.* 68 (2013) 1.
- [3] M. Ashby, *Scr. Mater.* 68 (2013) 4.
- [4] H.N.G. Wadley, *Philos. Trans. R. Soc. A* 364 (2006) 31.
- [5] T.A. Schaedler, A.J. Jacobsen, A. Torrents, A.E. Sorensen, J. Lian, J.R. Greer, L. Valdevit, W.B. Carter, *Science* 334 (2011) 962.
- [6] J.-H. Lim, K.-J. Kang, *Mater. Trans.* 47 (2006) 2154.
- [7] D. Erdeniz, A.J. Levinson, K.W. Sharp, D.J. Rowenhorst, R.W. Fonda, D.C. Dunand, *Metall. Mater. Trans. A* 46A (2015) 426.
- [8] L. Zhao, S. Ha, K.W. Sharp, A.B. Geltmacher, R.W. Fonda, A.H. Kinsey, Y. Zhang, S.M. Ryan, D. Erdeniz, D.C. Dunand, K.J. Hemker, J.K. Guest, T.P. Weihs, *Acta Mater.* 81 (2014) 326.
- [9] V.J. Challis, J.K. Guest, J.F. Grotowski, A.P. Roberts, *Int. J. Solids Struct.* 49 (2012) 3397.
- [10] S.H. Ha, J.K. Guest, *Struct. Multidiscipl. Optim.* 50 (2014) 65.
- [11] J.K. Guest, J.H. Prevost, *Int. J. Solids Struct.* 43 (2006) 7028.
- [12] M.V. Nathal, J.D. Whittenberger, M.G. Hebsur, P.T. Kantzos, D.L. Krause, Superalloy lattice block structures, in: K.A. Green, T.M. Pollock, H. Harada, T.E. Howson, R.C. Reed, J.J. Schirra, S. Walston (Eds.), *Superalloys 2004* (2004) pp. 431–439.
- [13] Q.M. Zhang, X.D. He, *Mater. Charact.* 60 (2009) 178.
- [14] L. Murr, S. Li, Y. Tian, K. Amato, E. Martinez, F. Medina, *Materials* 4 (2011) 782.
- [15] J.R. Rairden, M.R. Jackson, *J. Vac. Sci. Technol.* 17 (1980) 77.
- [16] G.W. Goward, L.W. Cannon, *J. Eng. Gas Turb. Power* 110 (1988) 150.
- [17] D. Erdeniz, D.C. Dunand, *Intermetallics* 50 (2014) 43.
- [18] M. Britchi, N. Ene, M. Olteanu, E. Vasile, P. Nita, E. Alexandrescu, *Defect Diffus. Forum* 297–301 (2010) 1.
- [19] F.S. Nogarani, F. Ashrafizadeh, A. Saatchi, *Surf. Coat. Tech.* 210 (2012) 97.
- [20] D.C. Dunand, D. Erdeniz, Transient liquid phase (TLP) bonding of nickel based alloys by forming an aluminum-titanium coating and subsequent heat treatment, U.S. Patent Office, App. No. 14/592,503 (2015).
- [21] G.P. Cammarota, A. Casagrande, G. Poli, P. Veronesi, *Surf. Coat. Tech.* 203 (2009) 1429.
- [22] G.O. Cook III, C.D. Sorensen, *J. Mater. Sci.* 46 (2011) 5305.
- [23] M.J. Donachie Jr (Ed.), *Superalloys Source Book*, ASM, Metals Park, OH, 1984.